Wind and Structures, Vol. 15, No. 1 (2012) 1-15
DOI: http://dx.doi.org/10.12989/was.2012.15.1.001

Wind characteristics of a strong typhoon in marine surface boundary layer

Lili Song[1], Q.S. Li*[2], Wenchao Chen[3], Peng Qin[3], Haohui Huang[3] and Y.C. He[2]

[1]*Guangzhou Institute of Tropical and Marine Meteorology, Guangzhou, 510080, China*
[2]*Department of Building and Construction, City University of Hong Kong, Hong Kong*
[3]*Guangdong Climate Centre, Guangzhou, 510080, China*

(Received January 16, 2011, Revised April 24, 2011, Accepted May 1, 2011)

Abstract. High-resolution wind data were acquired from a 100-m high offshore tower during the passage of Typhoon Hagupit in September, 2008. The meteorological tower was equipped with an ultrasonic anemometer and a number of cup anemometers at heights between 10 and 100 m. Wind characteristics of the strong typhoon, such as mean wind speed and wind direction, turbulence intensity, turbulence integral length scale, gust factor and power spectra of wind velocity, vertical profiles of mean wind speed were investigated in detail based on the wind data recorded during the strong typhoon. The measured results revealed that the wind characteristics in different stages during the typhoon varied remarkably. Through comparison with non-typhoon wind measurements, the phenomena of enhanced levels of turbulence intensity, gust factors, turbulence integral length scale and spectral magnitudes in typhoon boundary layer were observed. The monitored data and analysis results are expected to be useful for the wind-resistant design of offshore structures and buildings on seashores in typhoon-prone regions.

Keywords: strong typhoon; wind characteristic; wind data measurement.

1. Introduction

Typhoon is one of the most destructive natural disasters in the world, and could cause significant economic losses and heavy casualties every year. As reported by public media, when Typhoon Saomai slammed into China's southeastern coast in 2006, at least 460 people were killed and more than 60,000 houses and structures were destroyed, leading to a direct economic loss of exceeding RMB$ 23.8 billion. Unfortunately, typhoon-induced property damage, economic losses, and casualties have shown an increasing trend corresponding with population growth in the coastal regions of China and global warming phenomenon (Emanual 2005). Hence, it is necessary to understand typhoon-generated wind characteristics and improve current structural design codes of practice to address these design requirements.

More and more high-rise buildings and large-span structures have been built on seashores and the numbers of offshore platforms have been increased throughout the world in recent years. As such structures are sensitive to wind actions, it is thus required to systematically investigate the physical structures and characteristics of typhoons near seashores or in marine surface boundary layer for the

* Corresponding author, Dr., E-mail: bcqsli@cityu.edu.hk

wind-resistant design of these structures.

Studies on boundary layer characteristics of strong winds have been an important research topic in wind engineering all the time (Chow 1971, Ishizaki 1983, Naito 1988, Shiau 2000, Powell e*t al*. 2003, Schroeder and Douglas 2003, Wang and Wu 2004, Aberson *et al*. 2006). However, due to randomness of moving track and landing locations of typhoons, it is quite difficult to make elaborate observations of typhoon winds in the path of landfalling typhoons. In recent years, remote sensing systems, like RADAR (Knupp *et al*. 2005), SODAR (Tamura *et al*. 2007) and LIDAR (Antoniou *et al*. 2006), were adopted in the observations of wind characteristics during tropical cyclones or under non-typhoon wind conditions. These instruments have the ability of measuring wind data over a wide vertical range. But, they can hardly provide high-resolution wind data. Traditional anemometers still work as the main tool in various wind engineering fields, especially in the observation of wind characteristics in surface boundary layer.

In the last decade, a series of observation studies have been carried out on observation of typhoon winds in Hong Kong and Southeast China (Li *et al*. 2000, 2003, 2005, 2008, Pang *et al*. 2002, Song *et al*. 2005). But these studies were generally confined in coastal regions or inland areas. Boundary layer characteristics of typhoons in marine surface boundary layer were seldom reported. Therefore, there is an urgent need to conduct research works on this topic.

A 100-m high offshore meteorological tower with installation of numerous anemometers was established for investigating typhoon-generated wind characteristics in marine surface boundary layer in this study. It will be reported later that the centre of Typhoon Hagupit passed over the observation tower in September, 2008. Based on the high-resolution wind data recorded from the anemometers, this paper presents selected results of the wind characteristics during the strong typhoon, which are expected to provide useful information for further understanding typhoon-generated wind characteristics in marine surface boundary layer and for the wind-resistant design of offshore structures and buildings on seashores in typhoon-prone regions.

2. Data source and descriptions

2.1 Observation station

Bohe National Meteorological Observation Station (NMOS) consists of a 100-m meteorological tower which is located in an offshore island, a marine observation platform, and a wind profiler Doppler radar as well as meteorological anemometers on seashore. The guyed-mast tower is located at the highest site of an uninhabited island (21º26'20"N, 111º22'25"E)-Zhizai Island. The island which is of 90 m length, 40 width, 10 m height from the zenith to the sea level, and 4.5 km away from the nearest coastline, is oriented from northeast towards southwest and gradually bulges at the middle part. There are weeds surrounding the tower, while no large tree exists on the island. A wind observation system, comprised of several NRG-Symphonie cup-type anemometers, are installed on the tower: at the heights of 10 m, 20 m, 40 m, 60 m, 80 m and 100 m for wind speed monitoring; at the heights of 10 m, 60 m and 100 m for wind direction measurements, respectively. Besides, there is a Windmaster Pro 3-dimentional ultrasonic anemometer mounted at the height of 60 m of the tower (70 m above the sea level). Its maximum measurement capacity and sampling frequency are 65 m/s and 32 Hz, respectively. In this study, sampling frequency of 10 Hz was selected. The marine observation platform is located 1,500 m away from the east of Zhizai Island, which is equipped with

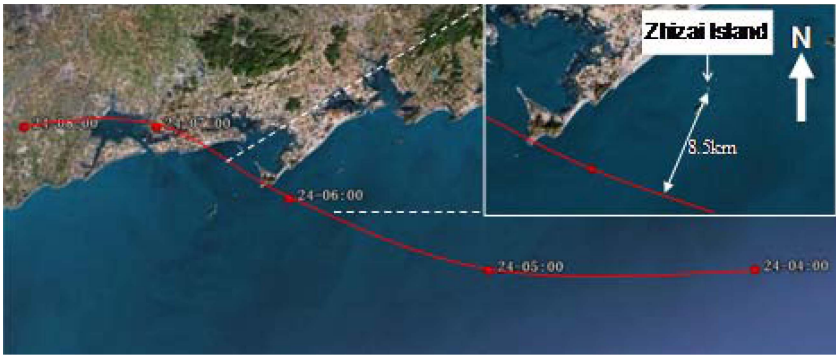

Fig. 1 Track of Typhoon Hagupit and location of the 100-m meteorological tower site

an observation system for wind speed and direction, relative humidity, air pressure and temperature. Fig. 1 shows the locations of the meteorological tower and the coastline.

2.2 Introduction of Typhoon Hagupit

Typhoon Hagupit formed as a tropical depression over northwest Pacific, about 2,540 km away from southeast Hong Kong, on the morning of Sep. 19th, 2008. It made landfall at Chen Village-a coastal village at Dianbai Town, Maoming City, Guangdong Province, at 6:45 am (Beijing time) on Sep. 24th. Typhoon Hagupit has been the strongest typhoon having ever landed in Guangdong in the last 14 years (after Typhoon Sally in 1996). According to the records from the Bohe meteorological station, the maximum 10 min mean wind speed was 48.5 m/s and the maximum 3 s gust speed was up to 63.9 m/s (at 60 m height on the island). The minimum air pressure was 956 hPa and lasted for 8 minutes from 05:18 to 05:25 on Sep. 24th. At Shangchuan Island national meteorological station, located about 150 km away from the typhoon eye, a maximum 3 s gust speed was recorded as 52 m/s. The track of the typhoon center is shown in Fig. 1, which was 8.5 km away from the southeast of Zhizai Island.

3. Wind data inspection and analyses

3.1 Data quality control procedures and stationary test

In this paper, the data samples were extracted from the original wind data records during 00:00 to 15:00 on Sep. 24th, 2008. The dataset was selected based on the following quality control procedures: (1) The anemometers were calibrated according to the clauses of "Near Surface Meteorological Observation Regulations in China"; (2) Wind data segments were eliminated in case of instrument mechanical failures or voltage irregularities (the anemometer at height of 80 m and the wind direction detecting instruments at heights of 10 m and 100 m were broken during the typhoon. Hence, the wind data from these equipments were excluded); (3) The ultrasonic anemometer was able to automatically distinguish invalid data caused by rainfalls. When selecting the data samples, invalid data were eliminated according to the discrimination code of the ultrasonic anemometer and were replaced by interpolation values. For each 10min data segment considered in

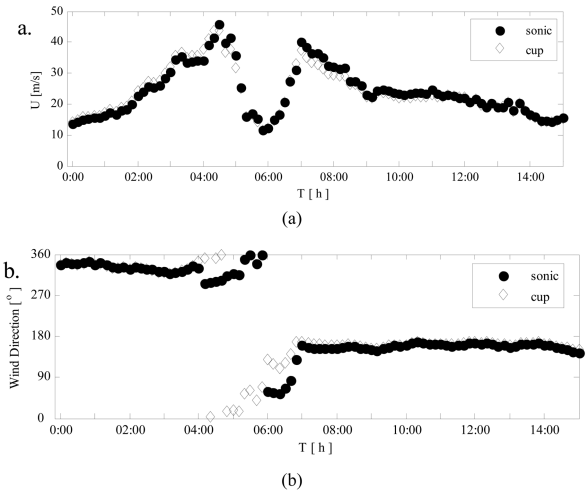

Fig. 2 10-min average wind speed and wind direction at height of 60m: (a) 10-min average wind speed and (b) 10-min average wind direction

this study, valid wind data should be no less than 98% for subsequent analysis.

To validate the quality of the wind data samples adopted in this study, 10 min mean wind speeds and wind directions from the ultrasonic anemometer are compared with those from the cup anemometer located at the same height (60 m). The comparison is presented in Fig. 2. As shown in the figure, variations of the wind speed and wind direction from the ultrasonic anemometer agreed well with those from the cup-type anemometer, verifying the accuracy and reliability of the two types of anemometers adopted in this study.

3.2 Typhoon representative data discrimination

It has been widely accepted that extreme winds in the eye-wall regions of typhoons are generally responsible for damages of buildings and structures. Hence, it is worthwhile to judge if the selected wind data samples were recorded when the eye-walls of the typhoon passed over the instrumented tower. According to the tropical cyclone hierarchy standard and typhoon wind characteristics, if the following two conditions are satisfied simultaneously, we can make sure that the typhoon centre did pass over the measurement station: (1) Wind speed variation of gale wind (10 min mean speed 17.2 m/s) during a typhoon process is distributed as an “M” shape with double-peaks. Meanwhile, when the typhoon eye is passing over the tower, the mean wind speed at the bottom part between the two peaks should be less than 11 m/s; (2) Wind direction of gale wind changes significantly. These two conditions were used in this study to judge the selected data samples corresponding to the different processes of the typhoon.

Fig. 3 depicts the variations of 10 min mean wind speed and wind direction during Typhoon Hagupit, in which the two green lines correspond to the time points of the two peak wind speeds occurred before and after the typhoon eye center passed over the instrumented tower; while the red line represents the time when the minimum wind speed was recorded (or when the typhoon eye center passed over the station). As can be seen, during the typhoon process, the gale wind speed was indeed distributed as an “M” shape with double-peaks, and the wind speed was also less than

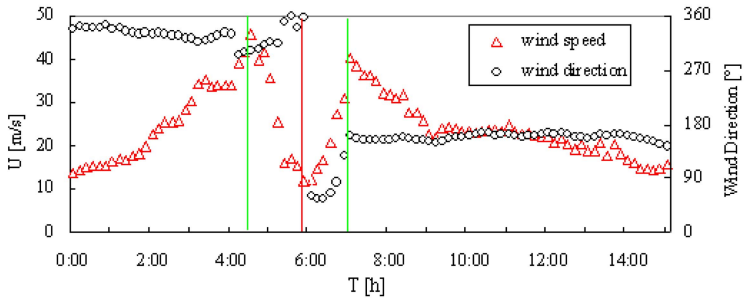

Fig. 3 10 min mean wind speed and direction of Typhoon Hagupit at 60 m height

11m/s at the bottom part between the two peaks. Meanwhile, the mean wind direction veered 182° during the typhoon. Hence, the selected typhoon records actually contained an integral dataset measured in the typhoon-eye and the eye-wall regions (commonly called 'cross-core typhoon'), and could represent the characteristics of Typhoon Hagupit.

3.3 Fluctuating wind data analysis

Instantaneous wind speed recorded by the ultrasonic anemometer at the height of 60 m on the tower was decomposed into longitudinal $u(t)$, transverse $v(t)$ and vertical $w(t)$ wind components in three orthogonal directions. The horizontal mean wind speed U, direction α, attack angle φ and the vertical mean wind speed W can be calculated by the following equations

$$U = \sqrt{\overline{u(t)}^2 + \overline{v(t)}^2} \tag{1}$$

$$\alpha = \arcsin\frac{\overline{u(t)}}{U} + step(-\overline{v(t)}) \times 180^{\circ} \tag{2}$$

$$\varphi = tg^{-1}(\overline{w(t)}/\overline{u(t)}) \tag{3}$$

$$W = \overline{w(t)} \tag{4}$$

where α equals 0^0 when wind blew from the north and 90^0 from the east; "step" denotes the step function.

The components of fluctuating wind speed in longitudinal, transverse and vertical directions $u'(t)$, $v'(t)$ and $w'(t)$, are computed as follows

$$u'(t) = u(t)\cos\alpha + v(t)\sin\alpha - U \tag{5}$$

$$v'(t) = -u(t)\sin\alpha + v(t)\cos\alpha \tag{6}$$

$$w'(t) = w(t) - W \tag{7}$$

4. Wind characteristics during the typhoon

4.1 Horizontal wind speed and direction

To supplement Fig. 3, the variation of the horizontal gust wind speed (0.1 s) from the ultrasonic anemometer is shown in Fig. 4. As can be seen, the first peak wind speed, arose before the passage of the typhoon center, blew from northwest with a 10min mean wind speed of 45.9 m/s and a 0.1 s gust speed of 63.9 m/s, respectively. The second one, occurred after the passage of the typhoon center, blew from southeast, corresponded to 40.1m/s and 60.2 m/s of the mean wind speed and gust speed, respectively. It was also observed that during the passage of the first eye-wall region, the gale wind (0.1s gust speed 50 m/s) lasted for about 50 minutes with the gust wind speed larger than 60 m/s for 19 times; while during the passage of the second eye-wall region, strength of the gale wind turned to be weaker with a shorter duration. On the whole, Typhoon Hagupit was stronger in the first eye-wall region. For the wind direction, as mentioned previously, it changed significantly from 351^0 before the passage of the typhoon center to 169^0 after the passage of the typhoon eye, with a variation of 182^0, indicating that the typhoon center passed over the instrumented tower.

4.2 Mean vertical wind speed and wind attack angle

Variations of 10 min average values of vertical wind speed and wind attack angle monitored during the typhoon are presented in Fig. 5. Meanwhile, the vertical mean wind attack angles of non-typhoon winds were also shown in this figure for comparison purposes. It was observed that vertical air nearly blew upward during the whole typhoon process. The vertical mean wind speed increased quickly in the eye-wall regions where the maximum value reached to 4.56 m/s. In the typhoon center, the upward flow was sharply weakened (there were even transient downward flows in the instantaneous records). In the peripheral regions, vertical wind angle characteristics were similar to those of non-typhoon winds. During Typhoon Hagupit, the vertical wind speeds recoded in the first eye-wall region were larger than those in the second eye-wall region. In other words, upward flows were stronger before the passage of the typhoon center. On the other hand, wind attack angle fluctuated during the typhoon. The first eye-wall region, featured by stronger wind speeds,

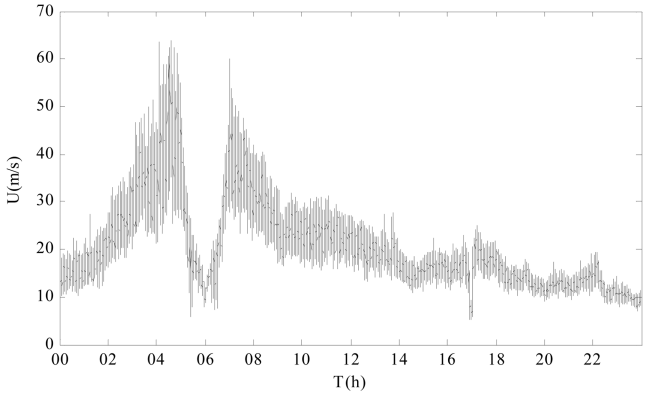

Fig. 4 Horizontal gust wind speed (0.1s) from the ultrasonic anemometer

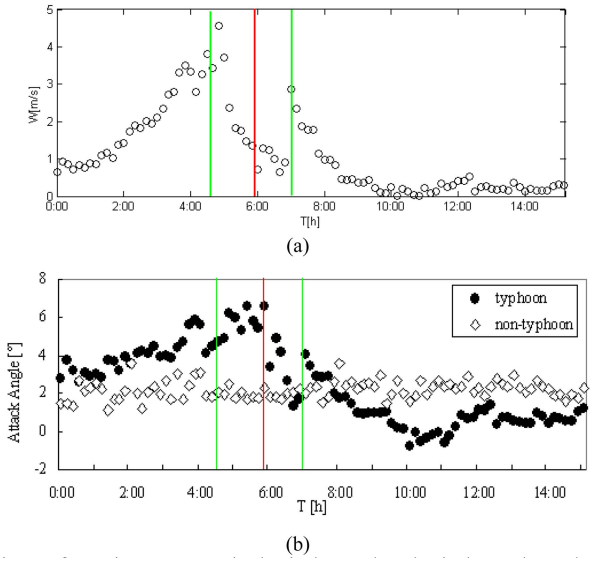

Fig. 5 Variations of 10 min mean vertical wind speed and wind attack angle at the height of 60 m during Typhoon Hagubit and non-typhoon winds. (a)Vertical wind speed and (b) wind attack angle

corresponded to larger positive values with a maximum one of 6.3°. This phenomenon may cause destructive consequences for civil structures since updraft winds could impinge upon decks of bridges, roofs of long-span buildings and low-rise buildings, resulting in damages of these structures. The peripheral regions corresponded to smaller attack angles which were similar to those of the non-typhoon winds. Compared to the results measured under non-typhoon winds, Typhoon Hagupit was characterized by much larger attack angles before the passage of the typhoon center.

4.3 Mean wind profiles

For neutrally stable atmospheric boundary layer, it is common to describe a wind speed profile with a power-law, such as in GB 50009-2001 (the code for building structure design in China), ASCE 7-05, and AIJ (Architectural Institute of Japan). The power-law is expressed as follows

$$u = u_1\left(\frac{z}{z_1}\right)^{\alpha} \tag{8}$$

where u and u_1 represent the wind speed at the height of z and z_1, α is the power exponent which reflects the roughness condition of the site. However, wind speed profiles under strong wind conditions may not follow the power-law completely (Li *et al*. 2009, 2010).

Fig. 6 displays the profiles of mean wind speed during Typhoon Hagubit, in which a profile was determined by 10 min wind speed data. The profiles varied with each other significantly: in the peripheral areas outside the eye-wall regions (1:30~4:20 and 8:30~15:00), the profiles were basically distributed exponentially. While inside the eye-wall regions (4:30~5:00 and 6:50~8:20), the profiles clearly deviated from the power-law. To make it clearer regarding the deviation, the profile of the maximum wind speed during the typhoon, which was measured at 4:30 in the first eye-wall

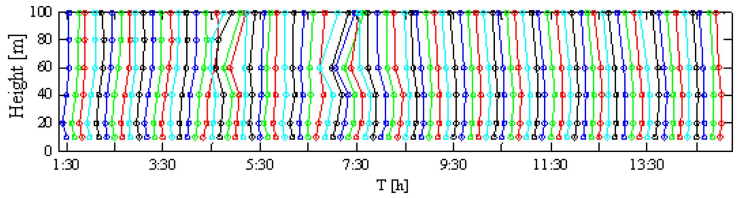

Fig. 6 Variation of 10 min mean wind speed profiles during Typhoon Hagubit

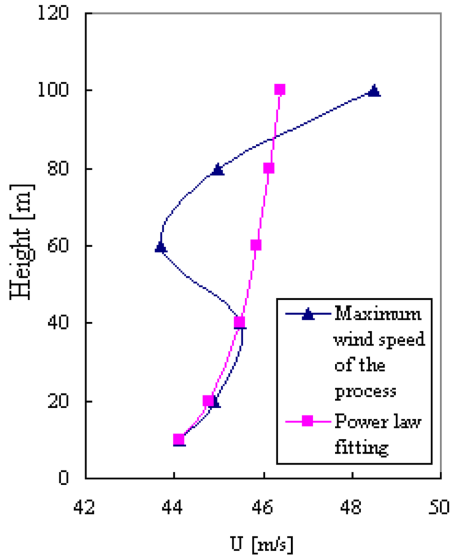

Fig. 7 The maximum 10 min mean wind speed profile during the typhoon

region, was extracted and presented in Fig. 7. The extracted wind speed profile obeyed the exponential curve quite well below 40 m. However, it differed remarkably from the power-law in higher altitudes.

It is interesting to note that all the non-exponential profiles trended alike. Wind speed increased rapidly below 40 m, but sharply decreased at the height of 60 m. This is obviously different from the ensemble mean wind speed profiles over deep ocean during hurricanes (Franklin *et al*. 2002) and under non-typhoon wind conditions on coastal regions (Tamura *et al*. 2007), in which the wind speed profiles showed a consistent exponential (or logarithmic) increase with altitude within the range mentioned above. The possible reason for this phenomenon may lie in the occurrence of negative shear transformation in lower boundary layer due to the special vortex structure of tropical cyclones (Wurman and Winslow 1998).

5. Turbulence characteristics

5.1 Turbulence intensity and gust factor

The turbulence intensity is defined as the ratio of the standard deviation of fluctuating wind to the mean wind speed of a given time span. It reflects the intensity of wind speed fluctuation, and is an

important parameter in the determination of wind-induced dynamic loads on buildings and structures. The equation for determining the parameter is given by

$$I_i = \frac{\sigma_i}{U}(i = u'(t), v'(t), w'(t)) \tag{9}$$

In this study, a 10 min time span was adopted to calculate turbulence intensities in the three orthogonal directions. Fig. 8 shows the variations of the turbulent intensity values based on the data measured from both the 3-dimentional ultrasonic anemometer and the cup type anemometer installed at the height of 60 m on the tower. The results of the longitudinal turbulence intensity from the two types of anemometers trended alike. But the values from the ultrasonic anemometer were generally a bit larger. This was mainly due to the different sampling frequencies of the two anemometers: 10 Hz for the ultrasonic anemometer and 1 Hz for the cup anemometer. Before the typhoon centre passed over the tower, the longitudinal turbulence intensity from the ultrasonic anemometer increased slightly, from 0.09 to 0.115; while those in the transverse and vertical directions changed little and were kept as 0.09 and 0.05, respectively. After the passage of the typhoon center, the turbulence intensity in each direction became smaller, with the value of 0.09, 0.07 and 0.04, respectively. On average, the proportion among the turbulence intensity in the three directions in the first eye-wall region was $I_u : I_v : I_w = 1 : 0.82 : 0.43$ and $I_u : I_v : I_w = 1 : 0.78 : 0.44$ in the second eye-wall region. On the other hand, the proportion was $I_u : I_v : I_w = 1 : 0.75 : 0.5$ in neutral surface boundary layer of non-typhoon winds (Counihan 1975). Thus, the enhanced level of the transverse turbulence intensity was observed, especially before the passage of the typhoon center.

Gust factor is another parameter to represent wind speed fluctuating characteristics. It is equal to the ratio of the peak gust wind speed $u_{\max}$ to the mean wind speed U, with the time spans of t and T for the gust speeds and the mean wind speed, respectively

$$G(t, T) = \frac{u_{max}(t)}{U(T)}, \; t < T \tag{10}$$

There are different choices of the time spans for determination of gust factor. In China, among many other countries, meteorologists and wind engineers commonly adopt $T = 10$ min and $t = 3$ s to determine gust factor which is called 3-second (3 s) gust factor.

The variation of the 3 s gust factor, obtained based on the data from both the ultrasonic and cup-type anemometers at the height of 60 m on the tower, is presented in Fig. 9. The values from the ultrasonic anemometer appeared larger than those from the cup-type anemometer mainly due to the

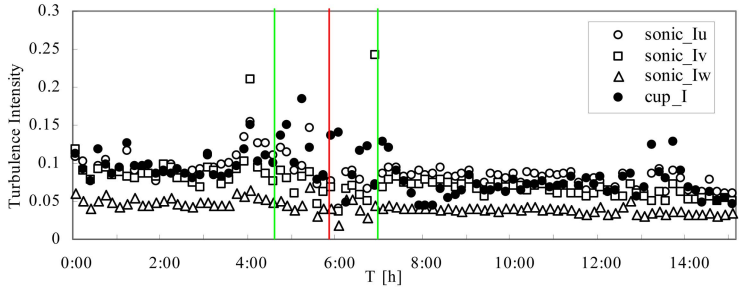

Fig. 8 Variation of turbulence intensity from the ultrasonic and cup anemometers at 60 m height

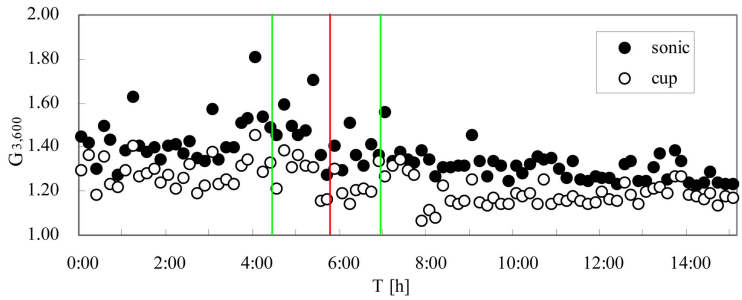

Fig. 9 Variation of gust factor from the ultrasonic and cup anemometers at 60 m height

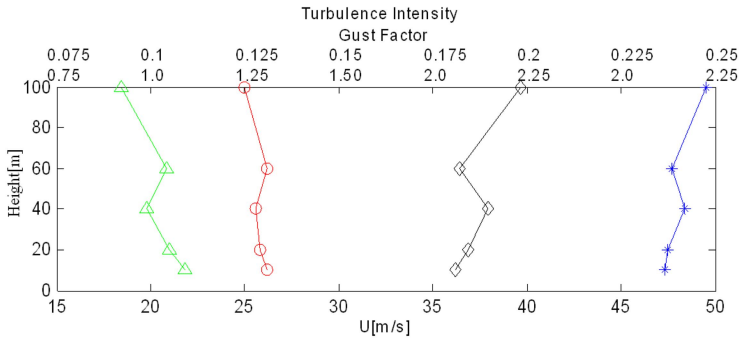

Fig. 10 Profiles of turbulence intensity, gust factor, mean wind speed and gust wind speed (◇ : 10 min mean wind speed, *: 3 s gust wind speed, ○ : gust factor, △ : turbulence intensity).

different sampling frequencies as mentioned previously, but they followed a similar tendency. The gust factor values increased in the eye-wall regions and were 3-7% larger than those in the peripheral areas. On average, the mean gust factors were 1.5 and 1.31 from the ultrasonic and cup anemometers, respectively, in the first eye-wall region, compared with 1.38 and 1.26 in the second eye-wall region.

Fig. 10 depicts the profiles of turbulence intensity, gust factor, mean wind speed and gust wind speed based on a 10 mins data sample with mean wind speed greater than 32.5 m/s (measured in the first eye-wall region). As can be seen from the figure, both the turbulence intensity and the gust factor values decreased substantially with altitude. At the height of 60 m, however, they changed sharply and made a visible increase, corresponding to the decrease of the wind speed at the same altitude, as discussed previously.

5.2 Turbulence integral length scale

It has been found that a length representing a sort of average eddy size in a turbulent flow is useful. The physical length used to quantify the turbulence gust is called the turbulence scale. There is more than one definition of this parameter. One of the most widely used scales is the integral length scale. Quantifying such parameters in extreme wind events is of interests to wind engineers, because information on the turbulence integral length scale in longitudinal, transverse and vertical directions is useful to determine the wind loads on a structure. Longitudinal turbulence integral

scale can be calculated using autocorrelation function method by Eqs. (11)-(13)

$$R_{u'u'}(\tau) = E[u'(t)u'(t+\tau)] \tag{11}$$

$$T_{um} = \frac{1}{\sigma_{u'}^2}\int_0^{\infty} R_{u'u'}(\tau)d\tau \tag{12}$$

$$L_{uu} = UT_{uu} \tag{13}$$

where $R_{u'u'}(\tau)$ is the autocorrelation function of longitudinal wind speed u' relative to a time lag value τ. In this paper, the upper limit of the integration in Eq. (12) used the time lag value when $R_{u'u'}(\tau)$ dipped below 0.05.

Fig. 11 shows the variation of the turbulence integral length scales in the longitudinal, transverse and vertical directions, which were determined based on the data from the ultrasonic anemometer. In the first eye-wall region, the values of the longitudinal turbulence scale increased with the wind speed and varied significantly from 130 m to 800 m. The peak value was 800 m at 4:00. The average longitudinal, transverse, vertical integral scales were 313 m, 206 m and 50 m, respectively. The proportion of the turbulence integral scale values in the three directions was L_{uu} : L_{vv} : L_{ww} = 1. : 0.66 : 0.16. Compared with those recommended by the guideline for bridge design in China (Xiang *et al*. 1996), the measured longitudinal turbulence integral scale was 2.6 times as larger as the suggested value, while the vertical integral scale was similar to the recommended value. After the typhoon center passed over the tower, the turbulence integral scale values in the second eye-wall region were similar to those in the peripheral regions, and the average longitudinal, transverse, vertical turbulence integral scales were 123 m, 137 m and 65 m, respectively. These results are different from those determined from Typhoon Wongfong and Typhoon Dujuan (Song *et al*. 2005) in which the turbulence integral length scale values increased evidently both before and after the passages of typhoon centers. Such differences may be caused by different terrain conditions where the measurements were made.

5.3 Power spectral density

Accurate prediction of structural response to wind loading requires an understanding of the distribution of wind energy with respect to frequency. In turbulent wind flows, larger size or low frequency eddies generate turbulent energy and smaller size or high frequency eddies dissipate it due to viscous effects. According to the Kolmogorov's hypotheses and Taylor's hypotheses

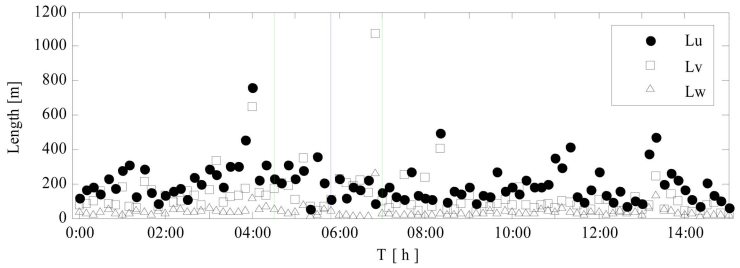

Fig. 11 Variations of the turbulence integral length scales from the ultrasonic anemometer

(Tieleman 1995), a spectrum of velocity fluctuation can be obtained based on dimensional consideration and experimentally determined coefficients

$$\frac{nS_a(n)}{u_*^2\phi_\varepsilon^{2/3}} = A_a f_z^{-2/3} \tag{14}$$

where n is frequency, $S_a(n)$ is the auto power spectral density (PSD), u_* is the friction velocity, ϕ_ε as a dimensionless dissipation rate for turbulence energy is a function of dimensionless height $\phi_\varepsilon = \frac{\varepsilon kz}{u_*^3}$, $A_a = a_a(2\pi k)^{-2/3}$, $k \approx 0.4$ is the von Karman constant, a_a is a universal constant (a_u=0.5, $a_v = a_w$=0.67), $f_z = nz/U$.

In the inertial sub-range, Simiu and Scanlan (1996) deduced a spectrum of longitudinal wind velocity as

$$\frac{nS_a(n)}{u_*^2} = 0.26 f_z^{-2/3} \tag{15}$$

The spectra of the longitudinal, transverse and vertical wind velocities measured from the ultrasonic anemometer during the typhoon and non-typhoon winds are presented in Fig. 12 for comparison purposes. It can be seen from Fig. 12(a) that the PSD under non-typhoon condition follows the Kolmogorov's law: i.e., assumption of isotropy is basically satisfied, $S_a(n)$ is proportional to $n^{-5/3}$ and the slope rate in the inertial sub-range is in accordance with the rule of −5/3 power. Figs. 12(a)-(d) represent the PSD distributions around and within the eye-wall regions.

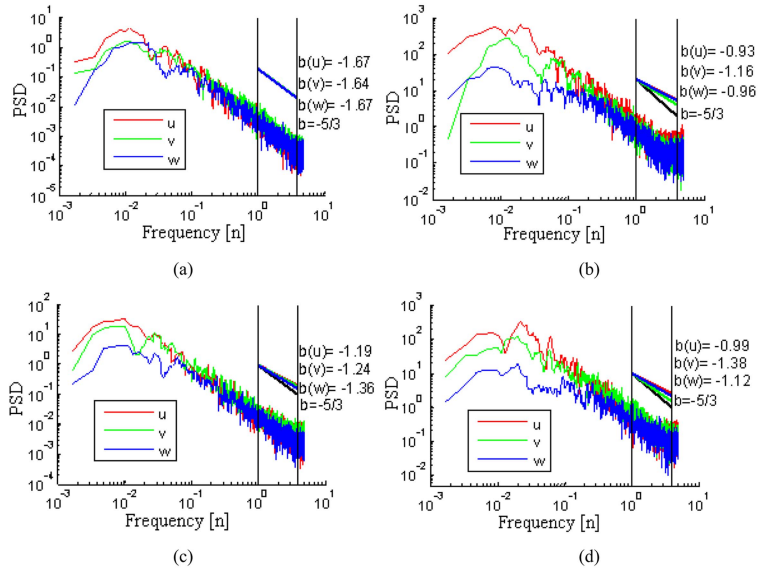

Fig. 12 Spectra of three wind components during the typhoon and non-typhoon winds (a) spectra of non-typhoon winds, (b) spectra in the eye-wall region before the passage of the typhoon center, (c) spectra in the typhoon eye center and (d) spectra in the eye-wall region after the passage of the typhoon center

Table 1. Average values of the PSD of the longitudinal, transverse and vertical wind components from the ultrasonic anemometer in three frequency ranges. (FEWR: in the first eye-wall region; SEWR: in the second eye-wall region, TE: in the typhoon eye, NT: in non-typhoon winds, $\overline{U}$: 10 min mean wind speed).

	Frequency range (Hz)								
	0.001-0.1			0.1-0.5			1-4		
Conditions	S_u	S_v	S_w	S_u	S_v	S_w	S_u	S_v	S_w
FEWR($\overline{U} \geq 32.7$ m/s)	117.252	77.065	10.665	5.689	4.876	2.443	0.206	0.195	0.158
SEWR($\overline{U} \geq 32.7$ m/s)	55.103	67.059	4.317	4.117	4.412	1.577	0.141	0.183	0.131
TE($\overline{U} \leq 15$ m/s)	9.978	5.009	1.253	0.623	0.420	0.234	0.135	0.0057	0.056
NT($\overline{U} = 6.1$ m/s)	0.919	0.849	0.329	0.032	0.028	0.026	0.001	0.001	0.001

These distributions in the inertial sub-range don't satisfy the isotropy assumption; neither does the slope rate in the inertial sub-range satisfy the −5/ 3 law. For the longitudinal wind velocity, the slope rate varies from −0.93 to −1.19, while the values for the transverse and vertical wind velocities change from −1.16 to −1.38 and −0.96 to -1.36, respectively.

Table 1 lists the PSD estimates of the longitudinal, transverse and vertical wind components measured in three different phases during Typhoon Hagupit (the first eye-wall region-FEWR, the second eye-wall region-SEWE, in the typhoon eye-TE, and in non-typhoon winds-NT). It can be observed from this table that in both the low-frequency and high-frequency ranges, turbulence energy in each direction in the two eye-wall regions was 1~2 order of magnitude larger than that in the typhoon center and that of non-typhoon winds. The longitudinal component values are larger than those in the transverse direction in the first eye-wall region before the passage of the typhoon center. But, the values in the transverse direction become larger than the longitudinal ones after the passage of the typhoon center. In non-typhoon conditions, by contrast, longitudinal PSD values are generally larger than the transverse ones.

6. Conclusions

This study investigated the wind characteristics of a strong typhoon on the basis of wind data records from an ultrasonic anemometer and a number of cup type anemometers installed on a 100 m offshore tower. Conclusions from this study are summarized as follows:

(1) Wind attack angle of typhoon wind was higher than that of non-typhoon wind. It increased with vertical wind speed. Such updraft flows during typhoons may impinge upon roofs of long-span buildings and decks of bridge, and may cause damages of these structures.

(2) The wind speed profiles in the eye-wall regions deviated from the power-law obviously. In the peripheral areas outside the eye-wall regions, the profiles were basically distributed exponentially.

(3) Turbulence intensity values in the longitudinal, transverse and vertical directions during the strong typhoon in marine surface boundary layer ranged from 9% to 15%, 9%-14% and 3%-8%, respectively, presenting a ratio of $I_u : I_v : I_w = 1 : 0.82 : 0.43$ before the passage of the typhoon center and $I_u : I_v : I_w = 1 : 0.78 : 0.44$ after the passage. The results were somewhat different from those measured in non-typhoon winds. The enhanced level of the transverse turbulence intensity was observed, especially before the passage of the typhoon center.

(4) The gust factor values increased in the eye-wall regions and were 3-7% larger than those in the peripheral areas.
(5) The turbulence integral length scales increased with wind speed. On average, the longitudinal, transverse and vertical turbulence integral length scales were 313 m, 206 and 50 m, respectively, with a proportion of $L_{uu} : L_{vv} : L_{ww} = 1 : 0.66 : 0.16$. The measured longitudinal value was 2.6 times as large as that recommended in the guideline for bridge design in China, while the vertical length scale value was similar to the suggested one.
(6) The spectra of typhoon winds around and inside the eye-wall regions did not satisfy the isotropy assumption and showed significant differences from those of non-typhoon winds. The spectra in inertial sub-range in the eye-wall regions remarkably deviated from the -5/3 law. The slope rates in the longitudinal, transverse and vertical directions changed from -0.93 to -1.19, -1.16 to −1.38 and −0.96 to −1.36, respectively. The measured spectra also show that the strong typhoon wind had more energy (1 or 2 order of magnitude higher) in the eye-wall regions than those in the peripheral areas and in non-typhoon winds. In the eye-wall region after the passage of the typhoon center, the transverse PSD values became larger than those in the longitudinal direction, while the opposite observation was made in the other processes of the typhoon. This was also different from the results obtained under non-typhoon wind conditions.

Acknowledgements

The work described in this paper was fully supported by two grants of National Natural Science Foundation of China (90715031, 40775071), a grant from the Research Grants Council of Hong Kong Special Administrative Region, China (Project No: CityU 117708) and a research grant from the Research Committee of City University of Hong Kong (Project No. 7002615).

References

Aberson, S.D., Black, M.L., Black, R.A., Burpee, R.W., Cione, J.J., Landsea. C.W. and Marks, F.D. (2006), "Thirty years of tropical cyclone research with the NOAA P-3 aircraft", *B. Am. Meteorol. Soc*., **87**, 1039-1055.
Antoniou, I., Jørgensen, H.E., Mikkelsen, T., Frandsen, S., Barthelmie, R., Perstrup, C. and Hurtig, M. (2006), "Offshore wind profile measurements from remote sensing instruments", *Proceedings of the European Wind Energy Association Conf. & Exhibition*, Athens.
Chow, S.H. (1971), *A study of the wind field in the planetary boundary layer of a moving tropical cyclone*, MS thesis, School of Eng. and Sci., N.Y. Univ., New York.
Counihan, J. (1975), "Adiabatic atmospheric boundary layers-a review and analysis of data from the period 1880-1972", *Atmos. Environ*., **9**(10), 871-905.
Emanual, K. (2005), "Increasing destructiveness of tropical cyclones over the past 30 years", *Nature*, **436**, 686-688.
Franklin, J.L., Black, M.L. and Valde, K. (2002), "GPS dropwindsonde wind profiles in hurricanes and their operational implications", *Weather Forecast*., **18**, 32-44.
Ishizaki, H. (1983), "Wind profiles, turbulence intensities and gust factors for design in typhoon-prone regions", *J. Wind Eng. Ind. Aerod*., **13**(1-3), 55-66.
Knupp, K.R., Walters, J. and Biggerstaff, M. (2005), "Doppler profiler and Radar observations of boundary layer variability during the landfall of tropical storm Gabrielle", *J. Atmos. Sci*., **63**(1), 234-251.
Li, Q.S., Fang, J.Q., Jeary, A.P., Wong, C.K. and Liu, D.K. (2000), "Evaluation of wind effects on a super tall

building based on full-scale measurements", *Earthq. Eng. Struct. D*., **29**(12), 1845–1862.
Li, Q.S., Xiao, Y.Q., Wong, C.K. and Jeary, A.P. (2003), "Field measurements of wind effects on the tallest building in Hong Kong", *Struct. Des. Tall Spec*., **12**(1), 67–82.
Li, Q.S., Xiao, Y.Q., and Wong, C.K. (2005), "Full-scale monitoring of typhoon effects on super tall buildings". *J. Fluid. Struct*., **20**(5), 697–717.
Li, Q.S., Xiao, Y.Q., Wu, J.R., Fu, J.Y. and Li, Z.N. (2008), "Typhoon effects on super-tall buildings", *J. Sound Vib*., **313**(3-5), 581–602.
Li, Q.S., Zhi, L.H. and Hu, F. (2009), "Field monitoring of boundary layer wind characteristics in urban area", *Wind Struct*., **12**(6), 553-574.
Li, Q.S., Zhi, L.H. and Hu, F. (2010), "Boundary layer wind structure from observation on a 325 m tower", *J. Wind Eng. Ind. Aerod*., **98**, 818-832.
Ministry of Construction of PRC, (2002), *Loading code for design of building structures GB50009-2001*, 72-74, China Construction Industry Press, Beijing.
Naito, G. (1988), "Turbulent properties and spectral behaviors of ocean winds observed at an offshore tower", *J. Wind Eng. Ind. Aerod*., **28**, 51–60.
Pang, J.B., Lin, Z.X. and Ge, Y.J. (2002), "Field measurements of strong wind characteristics near ground in Pudong district", Experiments and Measurements in Fluid Mechanics, **16**, 32-39.
Powell, M.D., Vickery, P.J. and Reinhold, T.A. (2003), "Reduced drag coefficient for high wind speeds in tropical cyclones", *Nature*, **422**, 279-283.
Schroeder J.L. and Douglas S. (2003), "A hurricane bonnie wind flow characteristics as determined from WEMITE", *J.Wind Eng. Ind. Aerod*., **91**(6), 767-789.
Shiau, B. (2000), "Velocity spectra and turbulence statistics at the northeastern coast of Taiwan under high-wind Conditions", *J. Wind Eng. Ind. Aerod*., **88**(2-3), 139-151.
Song, L., Hao, H. and Zhi, S. (2005), "Analysis on boundary layer turbulence features of land-falling typhoon", *Acta Meteorol. Sin*., **63**, 915-921 (in Chinese).
Simiu, E. and Scanlan, R.H. (1992), *Wind effects on structures: an introduction to wind engineering*, Wiley, New York.
Tamura, Y., Iwatani, Y., Hibi, K., Suda, K., Nakamura, O., Maruyama, T. and Ishibashi, R. (2007), "Profiles of mean wind speeds and vertical turbulence intensities measured at seashore and two inland sites using Doppler sodars", *J. Wind Eng. Ind. Aerod*., **95**(6), 411-427.
Tieleman, H.W. (1995), "Uinversality of velocity spectra", *J. Wind Eng. Ind. Aerod*., **56**, 55-69.
Wang, Y. and Wu, C.C. (2004), "Current understanding of tropical cyclone structure and intensity change-a review", *Meteor. Atmos. Phys*., **87**(4), 257-278.
Wurman, J. and Winslow J. (1998), "Intense sub-kilometer-scale boundary layer rolls observed in Hurricane Fran", *Science*, **280**(5363), 555-557.
Xiang, H.F., Lin, Z.X. and Bao W.G. (1996), *Guidelines for wind resistant design of bridges*, People's Transportation Press, Beijing.

CC